# *Regional atmospheric circulation over Europe during the Last Glacial Maximum and its links to precipitation*

AGU PUBLICATIONS

JGR

Journal of Geophysical Research: Atmospheres

RESEARCH ARTICLE
10.1002/2015JD024444

**Key Points:**
- Regional climate over Europe is analyzed under glacial conditions
- Precipitation patterns are strongly affected by the LGM large-scale atmospheric circulation
- Enhanced rainfall over Iberia is associated with enhanced oceanic evaporation and synoptic activity

**Supporting Information:**
- Figures S1–S7 and Table S1

**Correspondence to:**
P. Ludwig,
pludwig@meteo.uni-koeln.de

**Citation:**
Ludwig, P., E. J. Schaffernicht, Y. Shao, and J. G. Pinto (2016), Regional atmospheric circulation over Europe during the Last Glacial Maximum and its links to precipitation, *J. Geophys. Res. Atmos.*, *121*, 2130–2145, doi:10.1002/2015JD024444.

Received 3 NOV 2015
Accepted 12 FEB 2016
Accepted article online 18 FEB 2016
Published online 6 MAR 2016



# Regional atmospheric circulation over Europe during the Last Glacial Maximum and its links to precipitation

**Patrick Ludwig[1], Erik J. Schaffernicht[1], Yaping Shao[1], and Joaquim G. Pinto[1,2]**

[1]Institute for Geophysics and Meteorology, University of Cologne, Cologne, Germany, [2]Department of Meteorology, University of Reading, Reading, UK

**Abstract** The Last Glacial Maximum (LGM) exhibits different large-scale atmospheric conditions compared to present-day climate due to altered boundary conditions. The regional atmospheric circulation and associated precipitation patterns over Europe are characterized for the first time with a weather typing approach (circulation weather types, CWT) for LGM paleoclimate simulations. The CWT approach is applied to four representative regions across Europe. While the CWTs over Western Europe are prevailing westerly for both present-day and LGM conditions, considerable differences are identified elsewhere: Southern Europe experienced more frequent westerly and cyclonic CWTs under LGM conditions, while Central and Eastern Europe was predominantly affected by southerly and easterly flow patterns. Under LGM conditions, rainfall is enhanced over Western Europe but is reduced over most of Central and Eastern Europe. These differences are explained by changing CWT frequencies and evaporation patterns over the North Atlantic Ocean. The regional differences of the CWTs and precipitation patterns are linked to the North Atlantic storm track, which was stronger over Europe in all considered models during the LGM, explaining the overall increase of the cyclonic CWT. Enhanced evaporation over the North Atlantic leads to higher moisture availability over the ocean. Despite the overall cooling during the LGM, this explains the enhanced precipitation over southwestern Europe, particularly Iberia. This study links large-scale atmospheric dynamics to the regional circulation and associated precipitation patterns and provides an improved regional assessment of the European climate under LGM conditions.

## 1. Introduction

During the Last Glacial Maximum (LGM, about 21,000 years before present), the boundary conditions for the Earth's climate were drastically different from those of present-day. Variations in insolation due to orbital parameters [*Berger*, 1978], in topography due to ice sheet agglomeration [*Denton and Hughes*, 1981], and in trace gas compositions are considered to be the main drivers of atmospheric circulation differences during the LGM [e.g., *Kutzbach and Guetter*, 1986; *Pausata et al*., 2011; *Hofer et al*., 2012a, 2012b; *Löfverström et al*., 2014]. Their implications to the climate over Europe have been examined by means of various proxy data analyses. Pollen-based reconstructions by *Peyron et al*. [1998], *Tarasov et al*. [1999], and more recently *Bartlein et al*. [2011] revealed a general decrease of the mean annual temperature and precipitation over Europe. Based on speleothem analysis, *Luetscher et al*. [2015] suggested a potential reconstruction of the atmospheric circulation for the European Alps. Their proxy data records support the hypothesis of a southward shift of the North Atlantic storm track that in combination with enhanced moisture advection from the South explains the regional differences of a glacial ice buildup in the Alps. General circulation models (CGCMs) simulations provide additional insights into the large-scale LGM atmospheric circulation. The southward shift of the North Atlantic storm track during the LGM is also apparent in various paleoclimate simulations [*Kageyama et al*., 1999; *Laine et al*., 2009; *Pausata et al*., 2011], which results in enhanced precipitation over the Iberian Peninsula. This is in partial disagreement with the proxy data [*Bartlein et al*., 2011]. Thus, there is ongoing debate on the large-scale circulation and its regional implications (e.g., on precipitation) under different climate conditions [*Bony et al*., 2015; *Harrison et al*., 2015].

Climate model simulations allow for a better understanding of the atmospheric circulation under present and LGM boundary conditions. As pointed out by *Harrison et al*. [2015], CGCMs can generally simulate the changes in the large-scale circulation so that the regional climate presents the right anomalies, though they may not display the correct magnitude. Thus, the large-scale atmospheric circulation should be first considered when analyzing regional climate projections. For recent climate conditions, the North Atlantic Oscillation (NAO)

**Table 1.** List of Considered Models, Resolution of the Atmospheric Model, Considered Model Years, and Ensemble Code in PMIP3

| Model Name | Resolution (Atmosphere) | Model Years piControl | Model Years LGM | Ensemble Code |
|---|---|---|---|---|
| CCSM4 | 288 × 192 × L26 | 1063–1092 | 1870–1899 | r2i1p1 |
| MIROC-ESM | 128 × 64 × L80 | 2400–2429 | 4670–4699 | r1i1p1 |
| MPI-ESM-P | 196 × 98 × L47 | 2976–3005 | 1920–1949 | r1i1p1 |
| MRI-CGCM3 | 320 × 160 × L48 | 2321–2350 | 2570–2599 | r1i1p1 |

[e.g., *Hurrel et al*., 2003], characterized by the normalized pressure gradient of the Icelandic Low and the Azores High, has a strong influence on the climate in Europe, especially in the winter season. This pattern generally shows the well-known north-south mean sea level pressure (MSLP) dipolar structure in the historical time period [*Pinto and Raible*, 2012]. The NAO under the LGM conditions had a different structure with a more east-west alignment of the center of actions [*Justino and Peltier*, 2005, their Figure 3b], resulting in more meridional winds over the North Atlantic during the positive NAO phase. The findings of the latter authors are in agreement with the results of *Hofer et al*. [2012b], who analyzed atmospheric winter circulation types over the North Atlantic and Europe for preindustrial and glacial conditions (Marine Isotope Stage 4; MIS4). Their results indicate prevailing east-west MSLP patterns under glacial conditions, unlike the dominating north-south MSLP gradients for the recent climate. This leads to different precipitation patterns over Europe. Besides the NAO, the upper-level jet stream plays an important role in the Northern Hemisphere atmospheric circulation. *Oster et al*. [2015] demonstrated the relationship between of the location of semipermanent pressure systems over the Northern Pacific and the Laurentide Ice Shield (LIS) on the steering of the winter storm track toward western North America during the LGM. The changed circulation caused a shift of precipitation patterns, resulting in wetter conditions in southwestern North America and drier conditions close to the ice sheet. Over the North Atlantic, a more zonal and stronger upper-level jet stream is observed during the LGM in paleoclimate model simulations, in agreement with a stronger equatorial-pole temperature gradient [*Li and Battisti*, 2008]. Nevertheless, their simulations revealed less wind speed variability and a narrower latitudinal extend of the jet stream. The LGM mean state revealed also enhanced baroclinic instability [*Donohoe and Battisti*, 2009] and fewer cyclones, which play an important role in the poleward moisture transport and rainfall patterns. The authors argued that a stationary wave over the LIS, which steers upper-level disturbances poleward off the North Atlantic baroclinic zone, implies a reduced seeding of the upper-level jet, and thus, a decoupling of the North Pacific and North Atlantic storm tracks. Following these examples, a better understanding of regional and hemispheric circulation is essential to describe regional changes of, e.g., precipitation patterns.

The aim of our study is to characterize the regional atmospheric circulation for LGM conditions over Europe with a weather typing approach. We provide an improved regional assessment of the regional atmospheric circulation differences between the LGM and present-day over Europe and evaluate its implications on precipitation with regard to the large-scale atmospheric circulation (e.g., upper-level jet stream and storm tracks). This approach is in line with the current debate on the need for accelerated progress on the questions how jet stream, storm tracks, and precipitation interacts [*Bony et al*., 2015]. The regional circulation during the LGM is determined using the CWT approach after *Jones et al*. [1993]. This approach allows for a more regional analysis of the atmospheric circulation in addition to large-scale approaches, e.g., by *Hofer et al*. [2012b]. The CWTs have been extensively used in applications for recent and near future climate conditions in Europe [*Jones et al*., 2012; *Donat et al*., 2010], but not yet for paleoclimate conditions. Based on the weather type frequencies and associated precipitation intensities, we aim to explain the different mean precipitation patterns over Europe for present-day and LGM conditions and set them in context with large-scale atmospheric conditions.

## 2. Data and Methods

In this study, we use data from four atmosphere-ocean coupled general circulation models (CGCMs) that contributed to the third phase of the Paleoclimate Modeling Intercomparison Project (PMIP3) [*Braconnot et al*., 2012] (http://pmip3.lsce.ipsl.fr/). These models are (i) CCSM4 [*Gent et al*., 2011], (ii) MIROC-ESM [*Sueyoshi et al*., 2013], (iii) MPI-ESM-P [*Jungclaus et al*., 2013; *Stevens et al*., 2013], and (iv) MRI-CGCM3 [*Yukimoto et al*., 2012] (see Table 1 for additional information on individual models). The CGCM simulations follow the PMIP3 21 ka experimental design including blended ice sheet data by ICE-6G

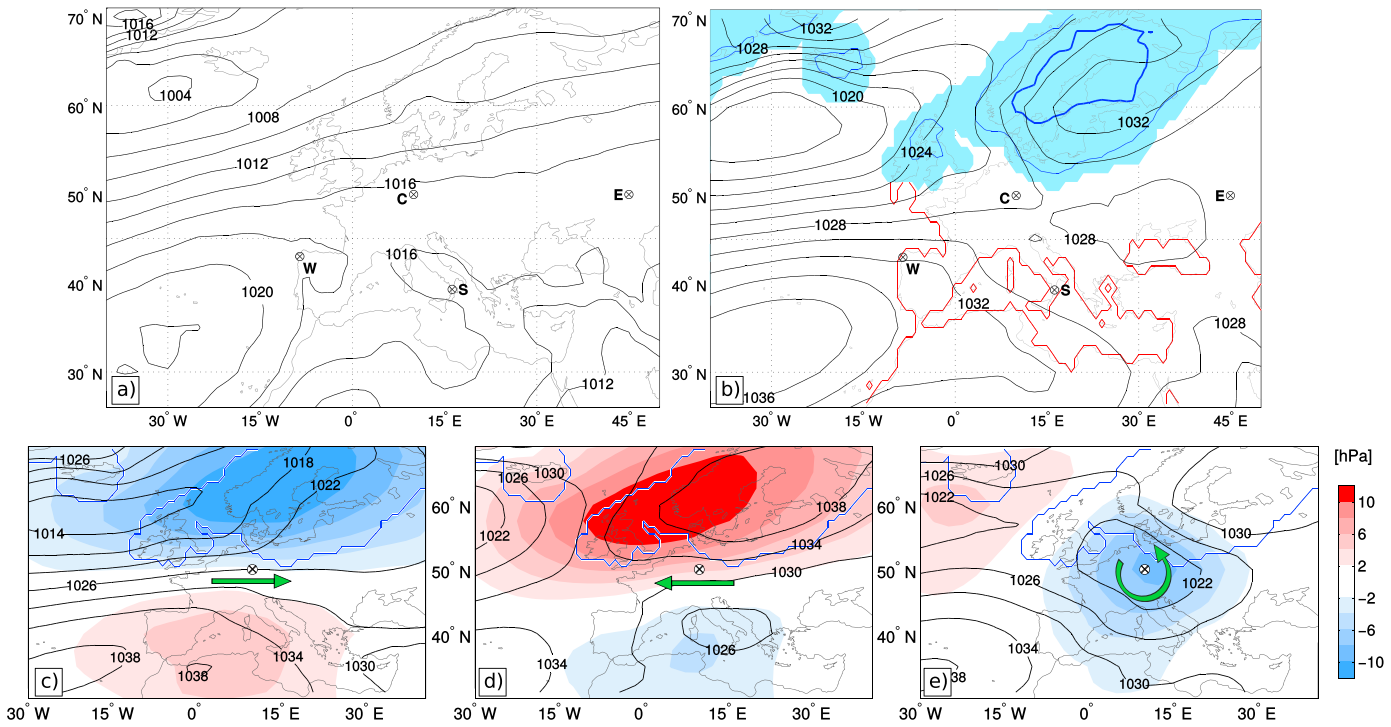


**Figure 1.** (a) Averaged MSLP from NCEP reanalysis (1970–1999, black lines, interval 2 hPa). (b) Averaged MSLP from PMIP3-LGM ensemble. Ice sheet extend (light blue) and height (thin blue line at 500 m, bold blue line 1500 m) of accumulated ice from blended ice sheet data by ICE-6G, ANU Ice Model, and GLAC-1 (see text for details). Red line denotes the boundary of 50% land fraction due to lower sea level at LGM. (Figures 1a and 1b) Locations of center grid points for the calculation of CWT frequencies at different locations across Europe: (C)entral, (W)est, (S)outh, and (E)ast. (c–e) Averaged MSLP from PMIP3-LGM ensemble (30 years, black lines, interval 4 hPa) and MSLP deviation from PMIP3-LGM ensemble mean (shaded areas) related to (Figure 1c) CWT West, (Figure 1d) CWT East, and (Figure 1e) CWT Cyclonic at the location Central (green arrow shows direction of flow). Blue line marks ice sheet extend at LGM.

[*Peltier et al.*, 2015], Australian National University (ANU) Ice Model [*Lambeck and Chappell*, 2001; *Lambeck et al.*, 2002], and GLAC-1 [*Tarasov and Peltier*, 2002, 2003] (see Figure 1b for ice sheet extend and additional land areas due to sea level decrease during the LGM). The last 30 year simulations of the steady PMIP3-LGM experiments (constant forcing) are compared with a 30 year period at the end of the steady PMIP3-piControl runs. The piControl runs are chosen to further assess the capabilities of the CGCMs to represent the present-day climate compared to National Centers for Environmental (NCEP)/National Center for Atmospheric Research (NCAR) reanalysis [*Kalnay et al.*, 2006]. Since the piControl runs are performed with constant (and weaker than present-day) greenhouse gas forcing, some slightly differences compared to NCEP/NCAR reanalysis might be expected. We use daily model data of mean sea level pressure and precipitation and monthly mean data for all other variables.

The regional atmospheric circulation is classified using the CWT approach after *Jones et al.* [1993]. The CGCM data are first interpolated to the regular 2.5° × 2.5° NCEP/NCAR grid. The prevailing wind direction is calculated around a central point using daily MSLP values of the surrounding 16 grid points [*Jones et al.*, 1993, Figure 1]. Here CWTs are calculated for four locations, referred to as West [43°N, 8.5°W], Central [50°N, 10°E], South [39°N, 16°E], and East [50°N, 45°E], which are representative of different climatic regions across Europe (Figures 1a and 1b). They help characterize the influence of the Atlantic Ocean (West), the effects of the Fennoscandian ice sheet (Central), the differences in the Mediterranean region (South), and in a continental climate (East). For all locations, except Central, a comparison of the CGCM results with proxy data is possible and helps the interpretation of the model results. For each location and day, the flow is classified into eight directional CWTs, namely, northeast (NE), east (E), southeast (SE), south (S), southwest (SW), west (W), northwest (NW), north (N), and two rotational CWTs, namely, cyclonic (C) and anticyclonic (A). Hybrid weather types are assigned to their corresponding directional CWT. Figures 1c and 1e show as example the pressure patterns associated with three CWTs (W, E, and C) at location Central for LGM conditions (see supporting information Figures S1–S4 for MSLP fields and anomalies for all CWTs and regions).

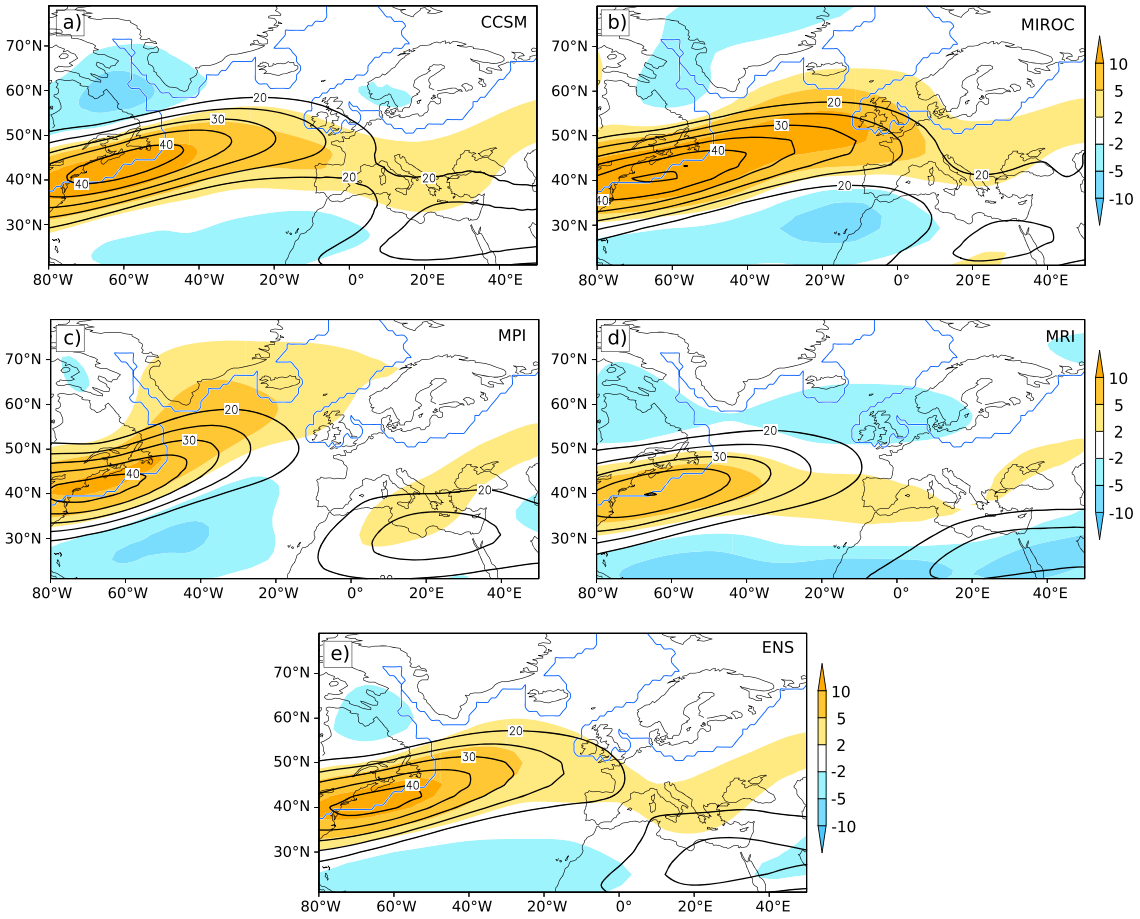


**Figure 2.** Annual mean of jet position and strength in simulations of the LGM climate (monthly wind speed averaged between 200 and 300 hPa, black contour lines each 5 m $s^{-1}$, starting at 20 m $s^{-1}$) over the North Atlantic and Europe. Shaded areas show differences between LGM and piControl for (a) CCSM, (b) MIROC, (c) MPI, (d) MRI, and (e) the ensemble mean (ENS). Blue line marks ice sheet extends at LGM.

The daily precipitation amount for each CWT is determined as the mean precipitation of the central grid point and its eight surrounding grid points. The precipitation data are also interpolated from the CGCM grid to the regular NCEP/NCAR grid. For both MSLP and precipitation, no bias correction has been performed in this study.

Following *Hoskins and Valdes* [1990], synoptic activity is quantified from the Eulerian perspective, as the variance of 2.5–6 day band passed filtered daily MSLP data. This variable is generally denominated storm track activity in the literature. Cyclone tracking (i.e., the Lagrangian tracking of individual low pressure systems, e.g., *Neu et al.* [2013]) is not performed in this study.

## 3. Results

### 3.1. Large-Scale Features Under Preindustrial and Glacial Conditions Over the North Atlantic-European Sector

Before considering the regional circulation over Europe, we examine the large-scale atmospheric conditions over the North Atlantic and Europe. The upper-level jet stream (here defined as the mean wind speed averaged between 200 and 300 hPa) is stronger in all models during the LGM compared to piControl (Figure 2). This is consistent with the results of *Li and Battisti* [2008]. For CCSM, MIROC, and MRI, a latitudinal narrowing and further extent toward continental Europe of the jet stream is obvious. While strength and differences between LGM and piControl are similar for CCSM and MIROC, the MRI model exhibits a weaker and more southward shifted jet stream. In contrast, the MPI model shows a stronger and broader jet stream toward the northeast of Europe and a slight strengthening of the LGM jet over southeastern Europe. Since the upper-level jet stream is strongly related to cyclone activity, we consider the North Atlantic storm track to

further assess differences of synoptic activity between LGM and piControl conditions. In general, the storm tracks of the piControl simulations agree with the observed storm track from NCEP data (Figure 3). Maximum activity is mainly simulated along and off the U.S. east coast and south of Greenland. CCSM shows an eastward shift of the maximum intensity toward southwest of Iceland. While the intensity of the storm track is underestimated in the MIROC model, it is overestimated for the MRI model. All models, and thus the piControl ensemble, show enhanced storm track activity over Europe. This can be explained by a generally more zonal atmospheric flow in CGCMs (not shown) and is related to the underrepresentation of atmospheric blocking over northern Europe in CGCMs [*Anstey et al*., 2013]. Over the northern parts of the North Atlantic, model results differ; while storm track activity is reduced for piControl compared to NCEP in the MIROC and MPI models, a slight increase can be observed for the CCSM and a strong increase of activity is simulated by MRI.

The storm tracks for the LGM generally show a stronger activity over Europe for all considered models [see also *Florineth and Schlüchter*, 2000; *Pausata et al*., 2011; *Löfverström et al*., 2014]. This is consistent with the eastward extension of the upper-level jet stream over Europe (Figure 2). For CCSM, MPI, and MRI, the increase of the storm track is mainly restricted south of the Scandinavian ice sheet, indicating its role of blocking the eastward passage of cyclones. However, an increase of the storm track occurs near Iceland and the Norwegian See is found for the MPI model. This is consistent with the strengthened upper-level jet stream over the northern parts of the North Atlantic. Unexpectedly, the storm track of MIROC is stronger over the Norwegian Sea and along the northern slopes of the Scandinavian ice sheet. Here the coarse resolution of the MIROC model compared to the other CGCMs is potentially accountable for this feature, as the actual ice sheet heights do have differences of several hundreds of meters (e.g., 2419 m for maximum over the Scandinavian ice sheet in MRI, 2029 m for MIROC). As shown in other studies, the height of the LIS plays an important role in governing the atmospheric circulation [e.g., *Hofer et al*., 2012a]. In case of coarse resolution, the orography of LIS becomes flatter and thus influences the resulting circulation over the North Atlantic and Europe. Additionally, the flattening of the Scandinavian ice sheet enables more cyclones to cross over this region. In the following, the influence of the altered large-scale features on the regional circulation is analyzed for different regions over Europe.

### 3.2. Regional Atmospheric Circulation Under Preindustrial and LGM Climate Conditions

To assess the capability of the CGCMs in simulating the circulation over Europe, we compare the CWT frequencies for the piControl CGCM ensemble (hereafter ENS_PI) and those derived from the NCEP/NCAR reanalysis. The climatological MSLP field depicts the semipermanent Icelandic Low and Azores High as main features (Figure 1a). A comparison of the CWT frequencies shows that the frequency of westerly CWTs is overestimated by the CGCMs over Central and Western Europe (Figures 4a and 4b), while the frequency of easterly CWTs is generally underestimated. This is consistent with more zonal orientated isobars of ENS_PI (Figure S5) and thus zonal atmospheric flow and is related to the underrepresentation of atmospheric blocking over northern Europe in CGCMs [*Anstey et al*., 2013]. For location South, the frequencies of SW to N CWTs are overestimated by all CGCMs while the eastern and southeastern CWT is underestimated (Figure 4c). For Eastern Europe, the CWT frequencies are in good agreement (Figure 4d), except for the slight overestimation of (south-) westerly at the expense of easterly flows. Moreover, the cyclonic (anticyclonic) CWT frequency is overestimated (underestimated). To summarize, the CGCMs generally reproduce well the observed CWT frequencies for present climate conditions, albeit some biases, which are comparable to those identified in other CGCM simulations [e.g., *Donat et al*., 2010].

The LGM MSLP field reveals essential differences to the present-day climate (Figure 1b): Under glacial conditions, the isobars over the North Atlantic Ocean are more zonally oriented which can be attributed to the more zonal jet stream in the LGM ensemble shown in Figure 2 (consistent with *Kageyama et al*. [2013a], *Löfverström et al*. [2014], and *Ullman et al*. [2014]). Furthermore, a cold high exists in northeastern Europe (Figure 1b) due to the buildup of the Fennoscandian ice shield [*Justino et al*., 2006]. At location West, the ENS_LGM and ENS_PI CWT frequencies are very similar (Figure 4a). Noticeable is the large model spread for the most frequent CWTs. While the MPI model simulates more frequent E but less frequent SW and W CWTs, the MIROC and CCSM models simulate enhanced frequent W and less frequent E CWTs. The decreased frequency of westerly CWTs in MPI is due to the northward shift of the upper-level jet stream, which is in contrast the other CGCMs (Figure 2). For Southern Europe, more frequent W and C CWTs are simulated for ENS_LGM and all individual models (Figure 4c). This is consistent with the (south-) eastward extent of the jet stream (Figure 2), the amplification of the North Atlantic storm track over this region (Figure 3), and the

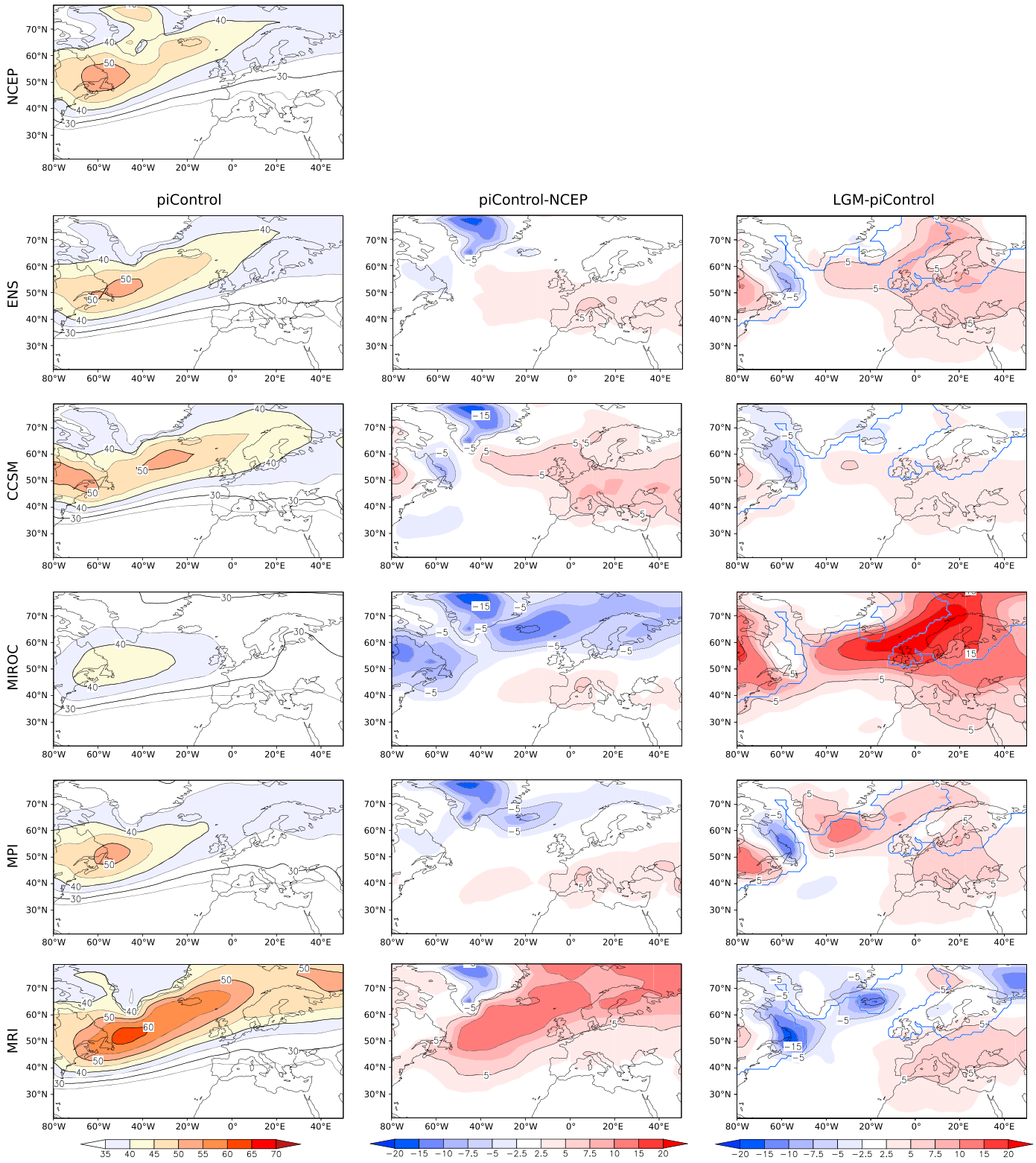


**Figure 3.** Storm tracks in simulations of the piControl and LGM climate (storm tracks 2.5–6 days band passed filter of daily MSLP data) for the PMIP3-piControl and LGM ensemble and individual models. (left column) storm tracks for NCEP and piControl simulations (1/10 hPa). (center column) Difference between piControl and NCEP (1/10 hPa). (right column) Storm track difference between LGM and piControl (LGM ice sheet extend marked by blue contour line).

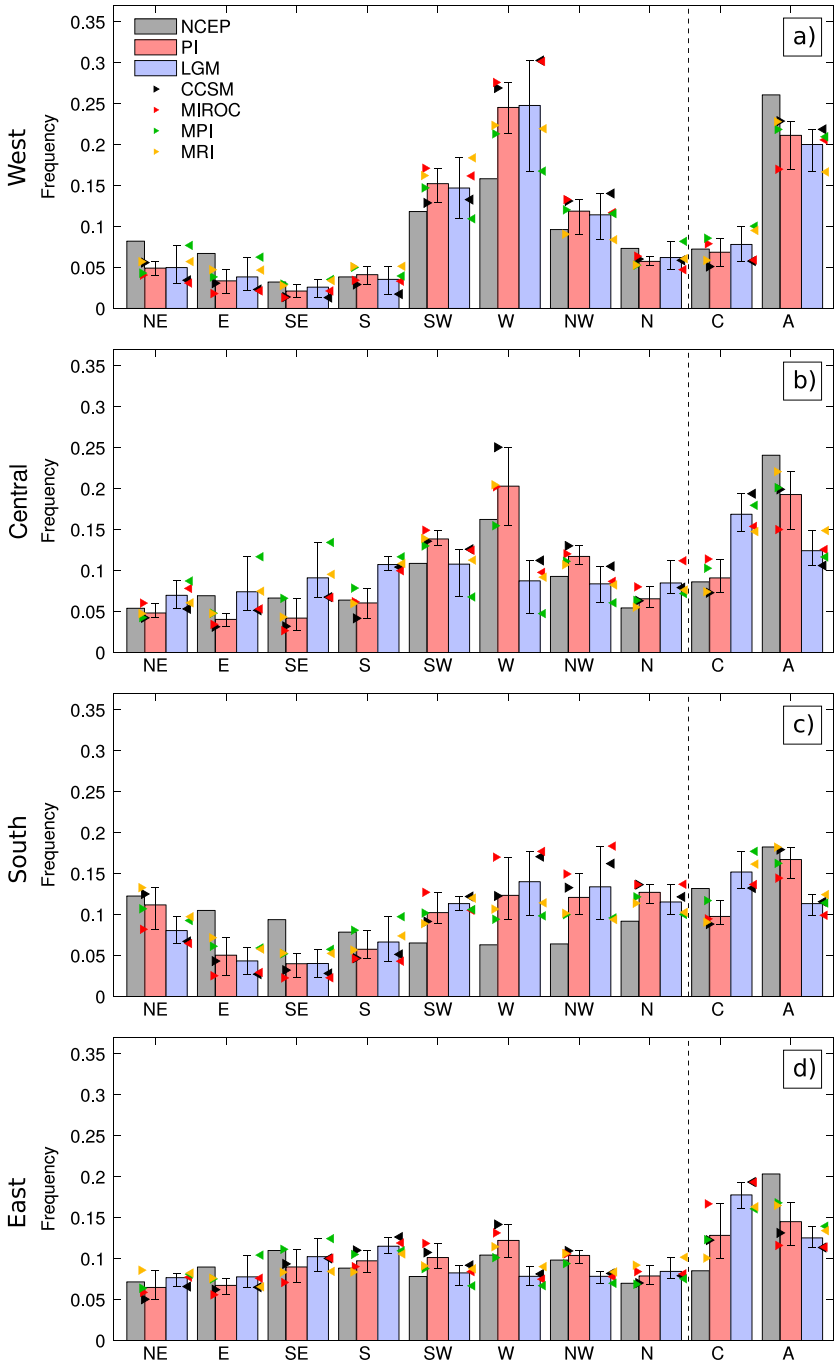


**Figure 4.** Comparison of CWT frequencies for piControl and LGM climate conditions for different locations across Europe (see Figure 1 for locations). (a) Western Europe, (b) Central Europe, (c) Southern Europe /Mediterranean, and (d) Eastern Europe. (Figures 4a and 4d) NCEP reanalysis data (grey), PMIP3-piControl ensemble mean (ENS_PI, red), and PMIP3-LGM ensemble mean (ENS_LGM, blue). Model spread (error bars) and deviations of individual PMIP3 models are also included (see color code for model assignment in Figure 4a).

hypothesized increase of cold air outbreaks over the western Mediterranean basin [*Kuhlemann et al.*, 2008]. For Central Europe, the changes of CWT frequencies are remarkable (Figure 4b), depicting a strong shift from W CWTs in ENS_PI to E and S CWTs for ENS_LGM. The enhanced frequency of E CWTs during LGM can be attributed to the changed boundary conditions (e.g., modified Fennoscandian ice sheet) and the resulting glacial anticyclone. The enhanced frequency of S and C CWT during LGM can be attributed to the southward displacement of both the jet stream [*Merz et al.*, 2015] and storm track, and a split of the storm track over the

Adriatic Sea, with one branch located north and east of the Alps [see *Florineth and Schlüchter*, 2000, Figure 6]. Likewise, cyclones are apparently constrained to move along the southern flank of the Fennoscandian ice sheet, which effectively blocks their passage northeastward. This also leads to an increase of the cyclonic frequency in all models. For Eastern Europe (Figure 4d), a slight decrease of all westerly CWT frequencies is observed for ENS_LGM, while all other CWT frequencies increase. The spread between the individual models is much lower at this continental location.

The seasonal changes between ENS_PI and ENS_LGM CWTs are analyzed for the four locations (Figure S6). In general, CWT frequencies vary strongly between summer and winter at all locations for both ENS_PI and ENS_LGM. For Western Europe, the CWT distributions are similar for all seasons in both ENS_PI and ENS_LGM. For Central Europe, a shift from NW and W (present) to S and E CWTs (LGM) is found in winter (Figure S6b). During summer (Figure S6j), the differences of the CWT frequencies are small. For Southern Europe, the ensemble means for all CWT frequencies in winter (Figure S6c) are almost identical. The general increase of the C CWT during the LGM over Southern Europe is associated with cold air outbreaks over the western Mediterranean basin [*Kuhlemann et al*., 2008]. Since the C CWT frequency hardly increases for summer (Figure S6k), it is assumed that the influence of these cold northerly air outbreaks is primarily restricted to the winter and transitional seasons. For Eastern Europe, a shift of SW, W, and NW CWTs toward increased northern and eastern CWTs is observed for LGM conditions during winter, spring, and autumn (Figures S6d, S6h, and S6p). For all four locations, the maximum spread among the individual models is generally lower during summer than in other seasons. The consideration of seasonal CWT distribution indicates that CWT frequencies are similar between ENS_PI and ENS_LGM during summer, while greater differences occur during the other seasons.

### 3.3. Regional Precipitation for Preindustrial and LGM Conditions

Under LGM conditions, southwestern Europe is wetter than today, while most of Scandinavia, Central, and Eastern Europe were much drier (see Figure 6). The mean daily precipitation amount related to each CWT for ENS_PI is first compared to NCEP/NCAR data. With this aim, daily precipitation on the central grid point and surrounding eight grid points is averaged for each location and assigned to the corresponding CWT. For almost all locations (except Southern Europe) and CWTs, a slight overestimation of the daily precipitation amount is observed for the CGCMs compared to NCEP (Figures 5a–5d). This is consistent with *Liu et al*. [2014], who compared summer and winter precipitation biases of the present-day CGCM simulations for central Europe. The CGCMs they investigated slightly underestimate summer precipitation but substantially overestimate winter precipitation. *Liu et al*. [2014] associated these precipitation biases to the general tendency of the climate models to producing light rainfall too often and heavy rainfall events too seldom [e.g., *Sillmann et al*., 2013]. The overestimation of light rainfall is associated with the unrealistic representation of the cloud microphysics, which is also the case for the CMIP5/PMIP3 CGCM simulations [*Liu et al*., 2014]. The situation is different for the Mediterranean basin (South), where an underestimation of some CWTs is identified. This is consistent with the results of *Perez-Sanz et al*. [2014, their Figure 4] who detected an underestimation of Mediterranean precipitation for three of the four CGCMs (CCSM4, MPI-ESM, and MIROC-ESM) considered in our study. *Perez-Sanz et al*. [2014] compared the preindustrial runs (piControl, appropriate for 1850 A.D.) to modern observations of the Climate Research Unit (CRU, *Harris et al*. [2014]) and detected only small differences.

The precipitation amounts associated with different CWTs for glacial conditions are now analyzed. The annual mean precipitation at each location depends on the CWT frequencies and the amount of precipitation associated with each CWT. A simple linear model is applied to the CWT frequencies and the associated precipitation amounts for both present-day and glacial conditions to explain the differences in the precipitation pattern over Europe (Figure 6a). Three combinations of CWT frequencies and precipitation intensities are considered: (a) historical CWT frequencies and rainfall intensities, (b) LGM CWT frequencies and historical rainfall intensities, and (c) LGM CWT frequencies and rainfall intensities. This can be written as

$$P_A = \sum_i P_i F_i,$$

where $P_A$ is the total precipitation, $P_i$ the precipitation attributed to CWT $i$ ($i$ = NE, E, …, N, C, AC), and $F_i$ is the frequency of the occurrence of CWT $i$.

The corresponding simulated annual precipitation at each location is depicted in Table 2 (upper part; see Table S1 for individual model precipitation). As shown in Table 2 (second row), the differences in CWT

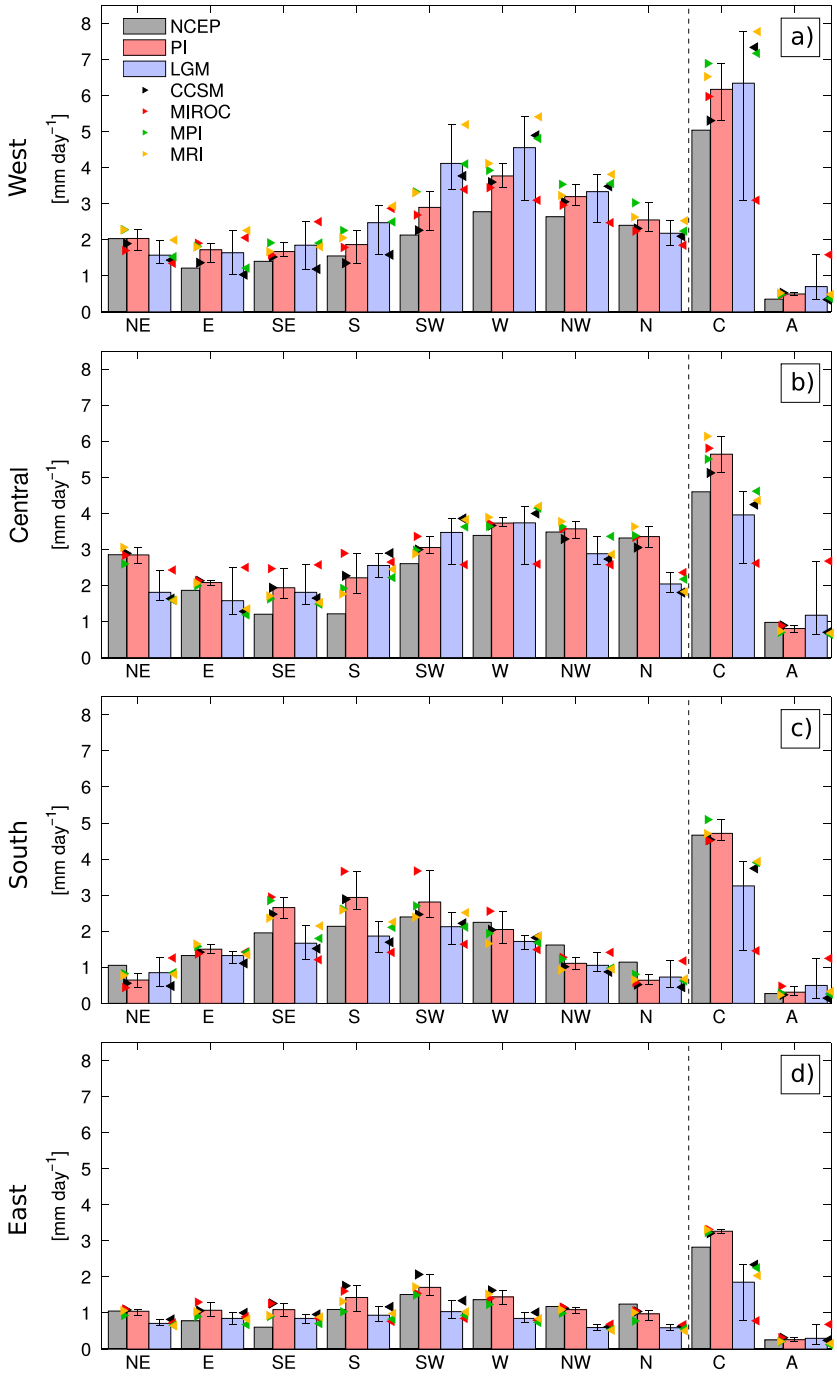


**Figure 5.** Comparison of mean precipitation (mm day$^{-1}$) for each CWT obtained from NCEP (grey), PMIP3-piControl ensemble (ENS_PI, red), and PMIP3-LGM ensemble (ENS_LGM, blue) for different locations across Europe ((a) Western Europe, (b) Central Europe, (c) Southern Europe /Mediterranean, and (d) Eastern Europe). Model spread (error bars) and deviations of individual PMIP3 models are also included (see color code for model assignment in Figure 5a).

frequencies cannot fully explain the precipitation differences between the LGM and present-day, as this leads to an increase of annual precipitation at all locations, whereas enhanced precipitation for LGM is only found over Western Europe (Figure 6a). This is largely related with the cyclonic CWT under LGM conditions: Over Western Europe, this CWT accounts for approximately 16% of the annual precipitation and it accounts for an even larger fraction over the other regions (Central: 26%, South: 31%, and East: 36%; cf. Table 2, lower part). While the cyclonic CWT is generally related to the largest precipitation intensities under current climate

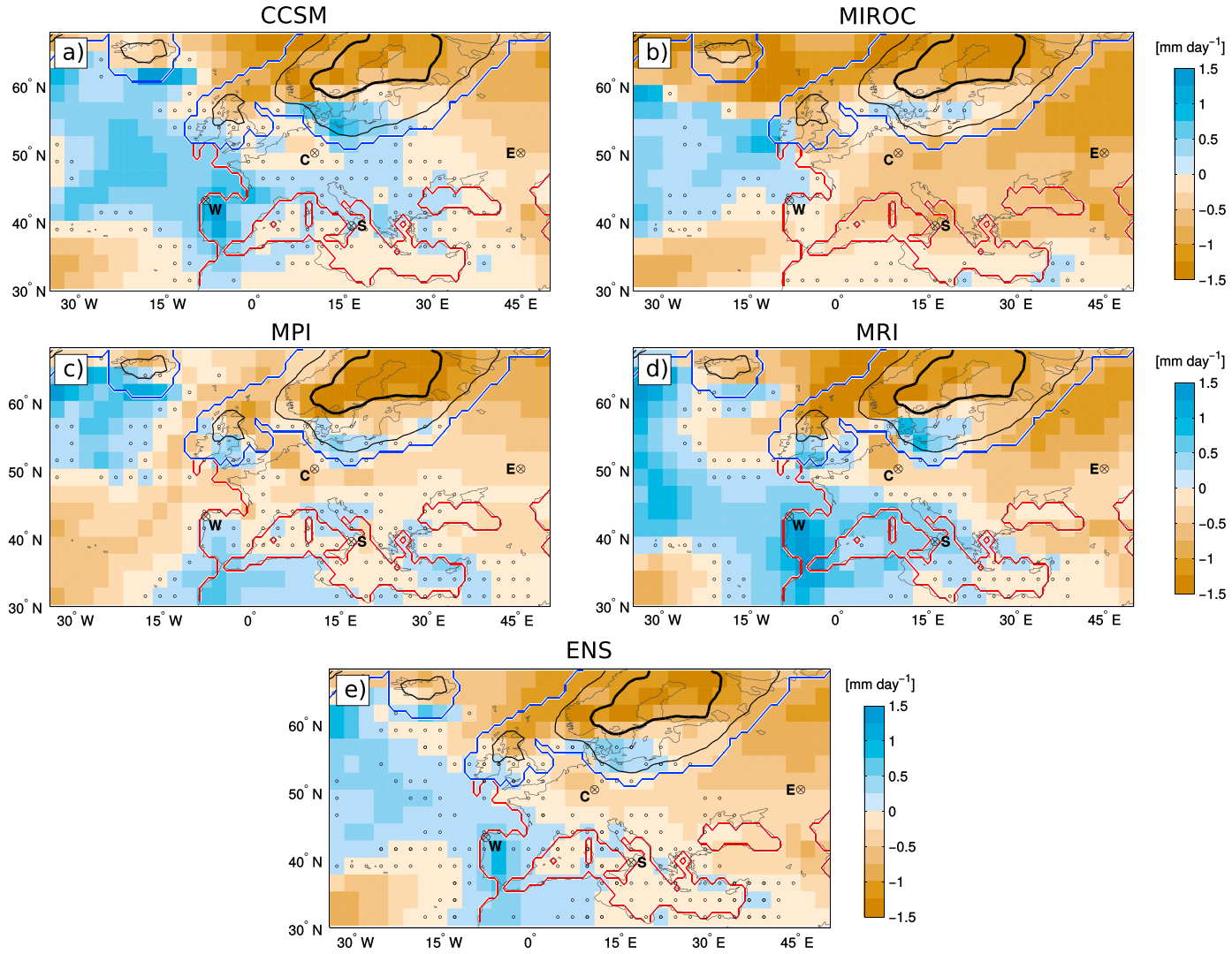


**Figure 6.** Differences between the daily mean precipitation in the PMIP3-LGM and the PMIP3-piControl ensemble for (a) CCSM, (b) MIROC, (c) MPI, (d) MRI, and (e) the ensemble mean (ENS) over Europe. LGM coastlines (red), LGM ice sheet (blue), and ice sheet height (thin black line at 500 m, bold black line at 1500 m) are shown. Grid points that are not statistically significant at the 5% level based on a two-sided Student's *t* test are marked by black circles. For the ensemble (Figure 6e) additionally two of the considered models must at least be significant for a grid cell to be considered significant within the ensemble.

conditions, the associated precipitation intensity is strongly reduced under LGM conditions. Thus, the differences in regional precipitation under LGM conditions can only be explained by a combination of both the different CWT frequencies and rainfall intensities per CWT.

Over Western Europe (Figure 5a), enhanced daily precipitation amounts are observed during the LGM for all CWTs except for N, NE, and E CWT. This agrees with enhanced mean daily precipitation over the Iberian Peninsula by up to 0.87 mm day$^{-1}$ (Figure 6e), which is a robust feature in simulations of the LGM [e.g., *Laine et al.*, 2009; *Hofer et al.*, 2012a, 2012b]. The highest increase of daily precipitation amounts can be found for SW and W CWTs. This corresponds to enhanced evaporation, and thus moisture advection, over the North Atlantic during glacial conditions (Figure 7). The individual models with the strongest increase of precipitation reveal the strongest increase of evaporation over the North Atlantic, which is in line with recent studies [*Hewitt et al.*, 2001; *Hofer et al.*, 2012b]. Over Central Europe (Figure 5b), an increase of daily mean precipitation for the LGM can be observed for W, SW, and S CWTs. This is true for all models (except MIROC) and can be attributed to the enhanced North Atlantic evaporation. Note that for MIROC only small areas with enhanced precipitation exist (Figure 7 b). In contrast, weaker mean daily precipitation occurs for all other directional CWTs, leading in

**Table 2.** Annual Mean Precipitation (mm year$^{-1}$) at Four Different Locations (West, Central, South, and East; see Figure 1) Based on Different Linear Combinations of CWTs and the Related Precipitation Intensities (RR) for piControl (PI) and Glacial (LGM) Conditions[a]

| | | West | Central | South | East |
|---|---|---|---|---|---|
| All CWTs | CWT-PI / RR-PI | 982 | 1066 | 617 | 502 |
| | CWT-LGM / RR-PI | 1000 | 1116 | 729 | 539 |
| | CWT-LGM / RR-LGM | 1152 | 953 | 575 | 340 |
| Cyclonic CWT excluded | CWT-PI / RR-PI | 827 | 879 | 449 | 349 |
| | CWT-LGM / RR-PI | 825 | 768 | 468 | 327 |
| | CWT-LGM / RR-LGM | 973 (16%) | 709 (26%) | 394 (31%) | 219 (36%) |

[a]The percentage given in the bottom row indicates the ratio of the precipitation for the cyclonic CWT compared to the total precipitation under LGM conditions. For more details see text.

combination with changing CWT frequencies to a total decrease of mean daily precipitation of up to 0.59 mm day$^{-1}$ for the LGM over central Europe. This strong reduction for northern and eastern CWTs can be attributed to much colder and drier conditions over the Fennoscandian ice sheet in LGM. For Southern and Eastern Europe (Figures 5c and 5d), weaker mean daily precipitation can be observed for almost all CWTs for glacial conditions. While this leads to generally weaker daily mean precipitation over large parts of Eastern Europe, only a slight decrease of precipitation (<0.1 mm day$^{-1}$) is observed for Southern Europe. The relatively small reduction of precipitation can be explained by enhanced

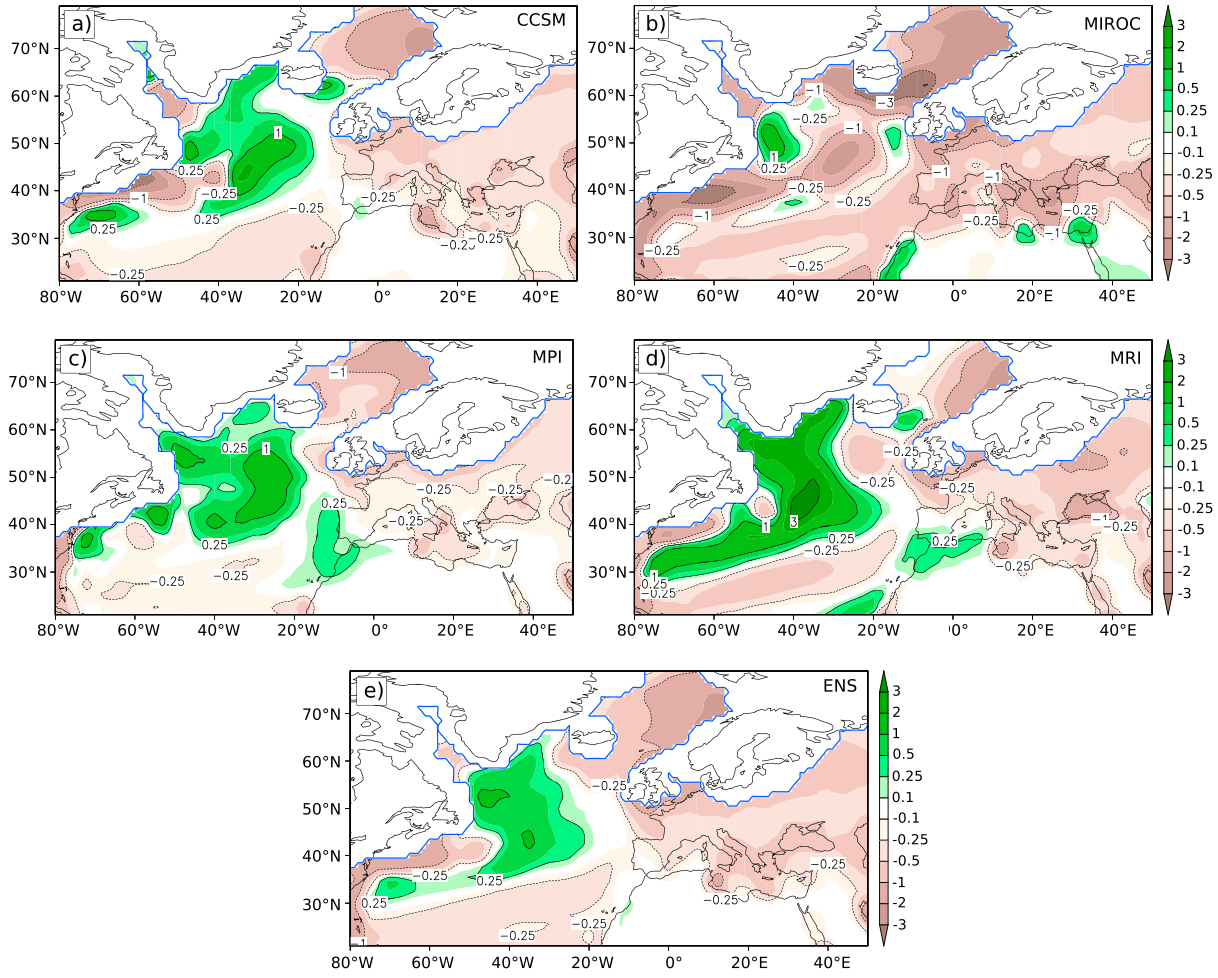


**Figure 7.** Differences between the evaporation in the PMIP3-LGM and the PMIP3-piControl ensemble based on monthly data (mm day$^{-1}$, ice sheets excluded). (a) CCSM, (b) MIROC, (c) MPI, (d) MRI, and (e) the ensemble mean (ENS). Blue line marks ice sheet extend at LGM (blue).

cyclone activity during the LGM (increase of CWT C, Figure 4c), which compensates the reduced precipitation by the other CWTs. The results of the precipitation differences partly disagree with proxy data. While the reduction of precipitation derived from proxy data agrees with less precipitation in CGCM simulations over Eastern Europe [*Tarasov et al*., 1999; *Bartlein et al*., 2011], enhanced rainfall over Western Europe is suggested by CGCM results that is not obvious from proxy data reconstructions [*Peyron et al*., 1998; *Bartlein et al*., 2011; *Moreno et al*., 2012].

We also consider the seasonal precipitation differences for each CWT for both present-day and LGM climate (Figure S7). The seasonal precipitation reveals differences depending on the season and the location (Table S2). The enhanced annual precipitation over Western Europe during LGM is related to stronger precipitation during winter and spring. The precipitation decrease over Central Europe is strongest during the transitional seasons of the LGM. While for Southern Europe stronger precipitation is found for the (relatively dry) summer, weaker precipitation is identified for the (relatively wet) autumn and winter. For Eastern Europe, all season show a reduction of precipitation during LGM, with strongest relative reduction occurring for summer. These seasonal precipitation changes can be primarily be attributed to the seasonal differences in terms of CWT frequencies (Figure S6).

A noticeable feature of the precipitation differences between present-day and LGM is the enhanced precipitation at the southern flank of the Fennoscandian ice sheet around 15°E (Figure 6), which is given by all considered CGCMs. A recap of main findings of this study helps to explain this feature. On the one hand, the W, SW, and W CWTs over Central Europe are associated with stronger precipitation due to enhanced evaporation over the eastern North Atlantic. Given the orographic lifting of air moving toward the Fennoscandian ice sheet, enhanced precipitation can be expected on the upwind slopes. A similar effect is found for the southern edge of the ice sheet over the British Isles. Another important point is the increase of S CWT over Central Europe, as consequence of the split of the storm track over the Adriatic Sea, with one branch extending north and east of the Alps. We conclude that both effects may have contributed to the buildup over time of the southern edge of the Fennoscandian ice sheet as suggested by *Florineth and Schlüchter* [2000].

### 3.4. Link Between Precipitation, Sea Surface Temperatures, and Evaporation

For CCSM, MPI, and MRI, enhanced precipitation especially over (south-) western parts of Europe is consistent with stronger evaporation over the North Atlantic (up to 3 mm day$^{-1}$ for MRI) and is consistent with earlier studies by *Hewitt et al*. [2001] and *Hofer et al*. [2012b]. The stronger evaporation in turn can be explained by a combination of enhanced surface wind speed and (for MPI and MRI) enhanced sea surface temperatures (SSTs) over parts of the North Atlantic Ocean. Figure 7 shows the differences between the SSTs between the LGM climate and piControl conditions together with the differences of the 10 m wind speed (for CCSM, 1000 hPa wind speed is used as no 10 m wind speed is available). All models show an increase of the 10 m wind speed for LGM conditions over central and eastern parts of the North Atlantic, which enhances evaporation. Additionally, the MPI and MRI reveal warmer SSTs over some parts of the North Atlantic Ocean that correspond to the regions of stronger evaporation. MIROC shows the strongest SST decrease along the considered models, which is consistent with reduced evaporation during LGM compared to piControl. An analysis of the Atlantic Meridional Overturning Circulation (AMOC) (following *Zhang and Wang* [2013] defined as the annual mean maximum meridional mass transport stream function below 500 m at 30°N) shows a strong increase for MPI and MRI (Figure 9). This explains the positive SST anomalies for these models at LGM conditions. A stronger AMOC for LGM condition has been recently identified in other coupled modeling studies [*Hewitt et al*., 2001; *Kageyama et al*., 2013b], although proxy data do not indicate a strengthening of the AMOC during the LGM [e.g., *McManus et al*., 2004; *Lynch-Stieglitz et al*., 2007].

## 4. Summary and Conclusions

The regional atmospheric circulation across Europe is analyzed for glacial (LGM) conditions based on a CGCM ensemble. Under LGM conditions, three of the four considered CGCMs show a stronger and eastward extended upper-level jet stream toward Europe, while a northward shift of the jet is found in the MPI-ESM. The response of the glacial storm tracks is in line with these upper-level changes: All models show enhanced storm track activity over Europe. This, together with changed boundary conditions over Europe, particularly the presence of the Fennoscandian ice sheet, helps to explain the regional circulation differences. While CWT frequency for Western Europe is comparable for recent climate and LGM conditions, this is not the case for the other three regions, where considerable differences are identified. A seasonal analysis for LGM conditions

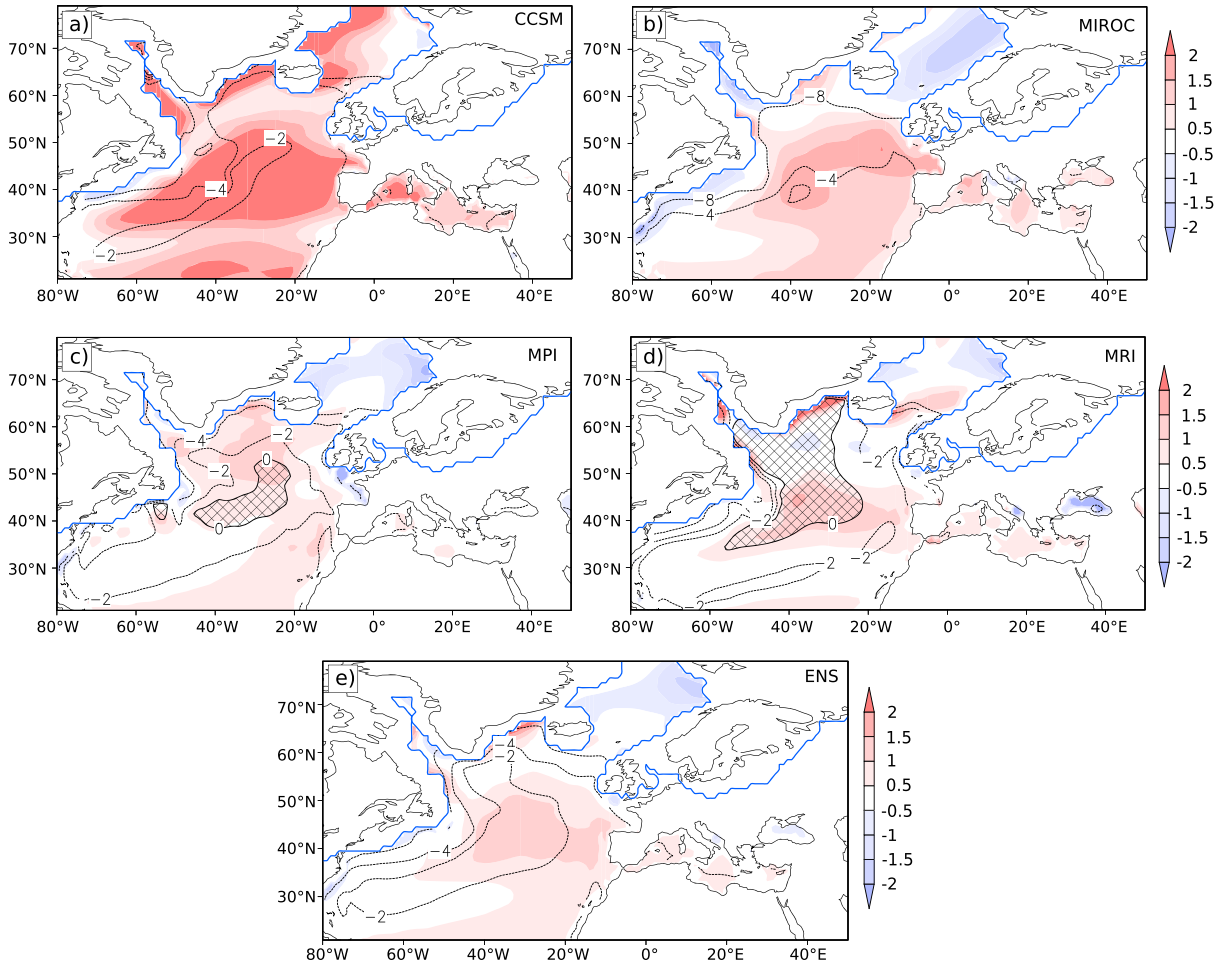


**Figure 8.** Differences between the SST (black contours, each 2°C; areas with higher SSTs during LGM hatched) and 10 m wind speed (m $s^{-1}$) (shaded) in the PMIP3-LGM and the PMIP3-piControl ensemble based on monthly data. For CCSM, wind speed at 1000 hPa is used, as no 10 m wind is available. (a) CCSM, (b) MIROC, (c) MPI, (d) MRI, and (e) the ensemble mean (ENS; wind speed mean only from MIROC, MRI, and MPI). Blue line marks ice sheet extend at LGM (blue).

reveals increased differences in CWT frequencies in all seasons except summer. Accordingly, the precipitation under LGM conditions displays enhanced precipitation over Western Europe for CCSM, MPI, and MRI and reduced precipitation over most of the remaining Europe for all models. The different precipitation patterns for LGM and present-day climate can be explained by a combination of changes in CWT frequencies and changes in mean precipitation per CWT. The enhanced mean precipitation is related to stronger evaporation over the North Atlantic Ocean for all models except MIROC. This in turn is associated with stronger near-surface wind speed and for two models (MPI and MRI) warmer SSTs. An analysis of the AMOC shows enhanced values of the ocean circulation for all models where data were available. Our analysis was limited to four models due to the current data availability in the CMIP5/PMIP3 database archive but could be improved if daily data are available for more models and more variables (e.g., geopotential height fields and moisture variables).

Based on this study, the following statements result for the regional circulation over Europe. For Western Europe, a slight increase of the (south-) westerly CWT frequencies is observed for the LGM. This is consistent with the earlier studies [e.g., *Hofer et al*., 2012b] and is consistent with a southern shift of the North Atlantic storm track (Figure 3) under the glacial conditions [see also *Laine et al*., 2009; *Pausata et al*., 2011; *Hofer et al*., 2012a]. The increase of precipitation over this area for LGM can be explained by stronger evaporation over the eastern North Atlantic (Figure 7), which is also described by *Hewitt et al*. [2001] and *Hofer et al*. [2012b]. This in turn is related to stronger surface wind speed and partly warmer SSTs over the North Atlantic (see Figure 8; MPI and MRI). Even though proxy data do not support a strengthening of the

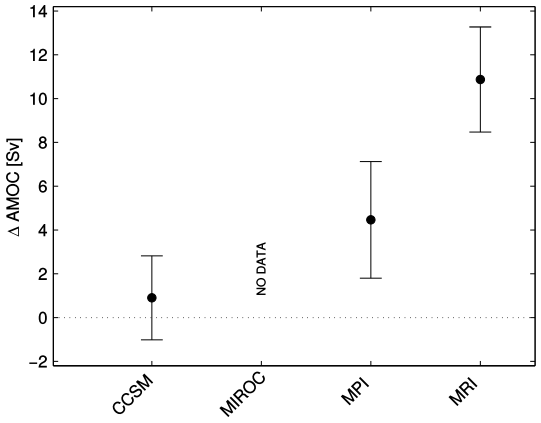


**Figure 9.** Differences between the AMOC (Sv) and standard deviation in the LGM and piControl simulations for models with data for AMOC available. AMOC is defined as the mean annual maximum of the meridional mass stream function at 30°N and between 500 and 1500 m depth for 30 years of LGM and piControl.

AMOC [*Lynch-Stieglitz et al*., 2007], the CGCMs do exhibit an increase of the AMOC for LGM (Figure 9), which has been identified for other coupled models [e.g., *Kageyama et al*., 2013b]. The most notable changes of CWT frequencies occurred in Central Europe, where a distinct shift from westerly (present-day) to southerly and easterly CWTs (LGM) is evident. This can be attributed to the buildup of the Fennoscandian ice sheet and the corresponding formation of a strong anticyclone. These findings are comparable to the leading patterns for glacial conditions found by *Hofer et al*. [2012b], where prevailing east-west MSLP patterns suggest similar changes of the mean atmospheric flow. Over Southern Europe, the most striking result is the strong increase of the cyclonic CWT frequency during the winter for LGM conditions. This can be attributed to enhanced cyclogenesis over the western Mediterranean associated with northern cold air outbreaks as described by *Kuhlemann et al*. [2008]. The analyses of CWTs for Central and Southern Europe also are in line with *Florineth and Schlüchter* [2000] regarding the buildup of the Fennoscandian ice sheet at its southern edge. An increase of mean daily precipitation for (south-) westerly CWTs over Central Europe and the split of the storm track over the Adriatic Sea, with one branch extending north and east of the Alps, are suggested to cause enhanced precipitation south to the ice sheet around 15°E. Finally, changes of CWT frequencies as well as the variability of the individual CGCM ensemble members are generally found to be less pronounced at Eastern Europe, where precipitation is largely reduced compared to recent climate conditions. The regional differences of the CWT distribution during the LGM are directly related with the large-scale conditions. The MPI model, showing a northward shift of the upper-level jet stream, simulates in general increased easterly CWT and less westerly flow frequencies at the considered regions (Figure 4). On the other hand, CCSM and MIROC (showing the strongest increase of the upper-level jet stream) simulate highest amounts for westerly and least easterly CWT frequencies. A general increase of the cyclonic CWT frequency during the LGM can be attributed to an extension of the North Atlantic storm track toward Europe.

Compared to terrestrial proxy data [e.g., *Peyron et al*., 1998; *Tarasov et al*., 1999; *Bartlein et al*., 2011; *Moreno et al*., 2012], the CGCM results point to enhanced precipitation during LGM conditions over Europe. Differences are largest over Western Europe where the considered models simulated enhanced rainfall compared to piControl. Our analysis provides a better understanding of the spread between the LGM model simulations and their agreement (or lack of) compared to the proxies, particularly over the Iberian Peninsula. As recently suggested by *Harrison et al*. [2015], improvements in the models are still necessary to better constrain their projections and thus produce more reliable regional projections for paleoclimate conditions.

**Acknowledgments**

We acknowledge the World Climate Research Programme's Working Group on Coupled Modelling, which is responsible for CMIP, and we thank the climate modeling groups (listed in section 2 of this paper) for producing and making available their model output.

For CMIP the U.S. Department of Energy's Program for Climate Model Diagnosis and Intercomparison provided coordinating support and led development of software infrastructure in partnership with the Global Organization for Earth System Science Portals. We thank Christoph Raible (University of Bern) for discussions as well as Daniel E. Ibarra (Stanford University) and two other anonymous reviewers for their comments on a previous version of this manuscript. This study is funded by the German Research Foundation (DFG) through the CRC 806 (Our way to Europe). The PMIP3 data are available from the PMIP3 homepage (https://pmip3.lsce.ipsl.fr/). The NCEP reanalysis data are available from the National Centers for Environmental Prediction (www.ncep.noaa.gov/). All other data and software are available from the authors on request (pludwig@uni-koeln.de).

## References

Anstey, J. A., P. Davini, L. J. Gray, T. J. Woollings, N. Butchart, C. Cagnazzo, B. Christiansen, S. C. Hardiman, S. M. Osprey, and S. Yang (2013), Multi-model analysis of Northern Hemisphere winter blocking: Model biases and the role of resolution, *J. Geophys. Res. Atmos.*, *118*, 3956–3971, doi:10.1002/jgrd.50231.

Bartlein, P. J., et al. (2011), Pollen-based continental climate reconstructions at 6 and 21 ka: A global synthesis, *Clim. Dyn.*, *37*, 775–802.

Berger, A. L. (1978), Long-term variations of daily insolation and Quaternary climatic changes, *J. Atmos. Sci.*, *35*, 2362–2367, doi:10.1175/1520-0469(1978)035<2362:LTVODI>2.0.CO;2.

Bony, S., et al. (2015), Clouds, circulation and climate sensitivity, *Nat. Geosci.*, *8*, 261–268.

Braconnot, P., S. P. Harrison, M. Kageyama, P. J. Bartlein, V. Masson-Delmotte, A. Abe Ouchi, B. Otto-Bliesner, and Y. Zhao (2012), Evaluation of climate models using paleoclimate data, *Nat. Clim. Change*, *2*, 417–424, doi:10.1038/nclimate1456.

Denton, G. H., and T. J. Hughes (1981), *The Last Great Ice Sheets*, 484 pp., Wiley Interscience, New York.

Donat, M. G., G. C. Leckebusch, J. G. Pinto, and U. Ulbrich (2010), European storminess and associated circulation weather types: Future changes deduced from a multi-model ensemble of GCM simulations, *Clim. Res.*, *42*, 27–43.

Donohoe, A., and D. S. Battisti (2009), Causes of reduced North Atlantic storm activity in a CCSM3 simulation of the Last Glacial Maximum, *J. Clim.*, *22*, 4793–4808.
Florineth, D., and C. Schlüchter (2000), Alpine evidence for atmospheric circulation patterns in Europe during the Last Glacial Maximum, *Quat. Res.*, *54*, 295–308.
Gent, P. R., et al. (2011), The Community Climate System Model Version 4, *J. Clim.*, *24*, 4973–4991, doi:10.1175/2011jcli4083.1.
Harris, I., P. D. Jones, T. J. Osborn, and D. H. Lister (2014), Updated high-resolution grids of monthly climatic observations—The CRU TS3.10 Dataset, *Int. J. Climatol.*, *34*, 623–642, doi:10.1002/joc.3711.
Harrison, S. P., P. J. Bartlein, K. Izumi, G. Li, J. Annan, J. Hargreaves, P. Braconnot, and M. Kageyama (2015), Evaluation of CMIP5 palaeo-simulations to improve climate projections, *Nat. Clim. Change*, *5*, 735–743, doi:10.1038/nclimate2649.
Hewitt, C., A. Broccoli, J. Mitchell, and R. Stouffer (2001), A coupled model study of the last glacial maximum: Was part of the North Atlantic relatively warm? *Geophys. Res. Lett.*, *28*(8), 1571–1574, doi:10.1029/2000GL012575.
Hofer, D., C. C. Raible, A. Dehnert, and J. Kuhlemann (2012a), The impact of different glacial boundary conditions on atmospheric dynamics and precipitation in the North Atlantic region, *Clim. Past*, *8*(3), 935–949, doi:10.5194/cp-8-935-2012.
Hofer, D., C. C. Raible, N. Merz, A. Dehnert, and J. Kuhlemann (2012b), Simulated winter circulation types in the North Atlantic and European region for preindustrial and glacial conditions, *Geophys. Res. Lett.*, *39*, L15805, doi:10.1029/2012GL052296.
Hoskins, B. J., and P. J. Valdes (1990), On the existence of storm tracks, *J. Atmos. Sci.*, *47*, 1854–1864.
Hurrel, J. W., Y. Kushnir, G. Ottersen, and M. Visbeck (2003), *An Overview of the North Atlantic Oscillation: Climatic Significance and Environmental Impact*, *Geophys. Monogr. Ser.*, vol. 134, pp. 1–35, AGU, Washington, D. C., doi:10.1029/134GM01.
Jones, P. D., M. Hulme, and K. R. Briffa (1993), A comparison of lamb circulation types with an objective classification scheme, *Int. J. Climatol.*, *13*, 655–663.
Jones, P. D., C. Harpham, and K. R. Briffa (2012), Lamb weather types derived from reanalysis products, *Int. J. Climatol.*, *33*, 1129–1139.
Jungclaus, J. H., N. Fischer, H. Haak, K. Lohmann, J. Marotzke, D. Matei, U. Mikolajewicz, D. Notz, and J.-S. von Storch (2013), Characteristics of the ocean simulations in MPIOM, the ocean component of the MPI Earth System Model, *J. Adv. Model. Earth Syst.*, *5*, 422–446, doi:10.1002/jame.20023.
Justino, F., and W. R. Peltier (2005), The glacial North Atlantic Oscillation, *Geophys. Res. Lett.*, *32*, L21803, doi:10.1029/2005GL023822.
Justino, F., A. Timmermann, U. Merkel, and W. R. Peltier (2006), An initial intercomparison of atmospheric and oceanic climatology for the ICE-5G and ICE-4G models of LGM paleotopography, *J. Clim.*, *19*, 3–14, doi:10.1175/JCLI3603.1.
Kageyama, M., P. J. Valdes, G. Ramstein, C. Hewitt, and U. Wyputta (1999), Northern Hemisphere storm tracks in present day and Last Glacial Maximum climate simulations: A comparison of the European PMIP models, *J. Clim.*, *12*, 742–760, doi:10.1175/1520-0442(1999)012<0742:NHSTIP>2.0.CO;2.
Kageyama, M., et al. (2013a), Mid-Holocene and Last Glacial Maximum climate simulations with the IPSL model—Part I: Comparing IPSL_CM5A to IPSL_CM4, *Clim. Dyn.*, *40*, 2447–2468.
Kageyama, M., et al. (2013b), Mid-Holocene and last glacial maximum climate simulations with the IPSL model: Part II: Model-data comparisons, *Clim. Dyn.*, *40*, 2469–2495.
Kalnay, E., et al. (2006), The NCEP/NCAR 40-year reanalysis project, *Bull. Am. Meteorol. Soc.*, *77*, 437–471.
Kuhlemann, J., E. J. Rohling, I. Krumrei, P. Kubik, S. Ivy-Ochs, and M. Kucera (2008), Regional synthesis of mediterranean atmospheric circulation during the Last Glacial Maximum, *Science*, *321*, 1338–1340, doi:10.1126/science.1157638.
Kutzbach, J. E., and P. J. Guetter (1986), The influence of changing orbital parameters and surface boundary-conditions on climate simulations for the past 18000 years, *J. Atmos. Sci.*, *43*(16), 1726–1759.
Laine, A., M. Kageyama, D. Salas-Melia, A. Voldoire, G. Riviere, G. Ramstein, S. Planton, S. Tyteca, and J. Y. Peterschmitt (2009), Northern Hemisphere storm tracks during the Last Glacial Maximum in the PMIP2 ocean-atmosphere coupled models: Energetic study, seasonal cycle, precipitation, *Clim. Dyn.*, *32*, 593–614, doi:10.1007/s00382-008-0391-9.
Lambeck, K., and J. Chappell (2001), Sea level change through the last glacial cycle, *Science*, *292*, 679–686, doi:10.1126/science.1059549.
Lambeck, K., Y. Yokoyama, and A. Purcell (2002), Into and out of the Last glacial Maximum sea level change during Oxygen Isotope Stages 3–2, *Quat. Sci. Rev.*, *21*, 343–360.
Li, C., and D. S. Battisti (2008), Reduced Atlantic storminess during the Last Glacial Maximum: Evidence from a coupled climate model, *J. Clim.*, *21*, 3561–3579.
Liu, Z., A. Mehran, T. J. Phillips, and A. AghaKouchak (2014), Seasonal and regional biases in CMIP5 precipitation simulations, *Clim. Res.*, *60*, 35–50, doi:10.3354/cr01221.
Löfverström, M., R. Caballero, J. Nilsson, and J. Kleman (2014), Evolution of the large-scale atmospheric circulation in response to changing ice sheets over the last glacial cycle, *Clim. Past*, *10*, 1453–1471, doi:10.5194/cp-10-1453-2014.
Luetscher, M., R. Boch, H. Sodemann, V. Spötl, H. Cheng, R. L. Edwards, S. Frisia, V. Hof, and W. Müller (2015), North Atlantic storm track changes during the Last Glacial Maximum recorded by Alpine speleothems, *Nat. Commun.*, *6*, 6344, doi:10.1038/ncomms7344.
Lynch-Stieglitz, J., et al. (2007), Atlantic meridional overturning circulation during the Last Glacial Maximum, *Science*, *316*, 66–69.
McManus, J. F., R. Francois, J.-M. Gherardi, L. D. Keigwin, and S. Brown-Leger (2004), Collapse and rapid resumption of Atlantic meridional circulation linked to deglacial climate changes, *Nature*, *428*, 834–837, doi:10.1038/nature02494.
Merz, N., C. C. Raible, and T. Woollings (2015), North Atlantic eddy-driven jet in interglacial and glacial winter climates, *J. Clim.*, *28*, 3977–3997, doi:10.1175/JCLI-D-14-00525.
Moreno, A., P. González-Sampériz, M. Morellón, B. L. Valero-Garcés, and W. J. Fletcher (2012), Northern Iberian abrupt climate change dynamics during the last glacial cycle: A view from lacustrine sediments, *Quat. Sci. Rev.*, *36*, 139–153.
Neu, U., et al. (2013), MILAST: A community effort to intercompare extratropical cyclone detection and tracking algorithms, *Bull. Am. Meteorol. Soc.*, *94*, 529–547, doi:10.1175/BAMS-D-11-00154.1.
Oster, J. L., D. E. Ibarra, M. J. Winnick, and K. Maher (2015), Steering of westerly storms over western North America at the Last Glacial Maximum, *Nat. Geosci.*, *8*, 201–205.
Pausata, F. S. R., C. Li, J. J. Wettstein, M. Kageyama, and K. H. Nisancioglu (2011), The key role of topography in altering North Atlantic atmospheric circulation during the last glacial period, *Clim. Past*, *7*(4), 1089–1101, doi:10.5194/cp-7-1089-2011.
Peltier, W. R., D. F. Argus, and R. Drummond (2015), Space geodesy constrains ice age terminal deglaciation: The global ICE-6G_C (VM5a) model, *J. Geophys. Res. Solid Earth*, *119*, 450–487, doi:10.1002/2014JB011176.
Perez-Sanz, A., G. Li, P. González-Sampériz, and S. P. Harrison (2014), Evaluation of modern and mid-Holocene seasonal precipitation of the Mediterranean and northern Africa in the CMIP5 simulations, *Clim. Past*, *10*, 551–568, doi:10.5194/cp-10-551-2014.
Peyron, O., J. Guiot, R. Cheddadi, P. Tarasov, M. Reille, J.-L. de Beaulieu, S. Bottema, and V. Andrieu (1998), Climatic reconstruction in Europe for 18 000 yr BP from pollen data, *Quat. Res.*, *49*, 183–196.

Pinto, J. G., and C. C. Raible (2012), Past and recent changes in the North Atlantic oscillation, *Wiley Interdiscip. Rev. Climate Change*, *3*, 79–90, doi:10.1002/wcc.150.

Sillmann, J., V. Kharin, X. Zhang, F. Zwiers, and D. Bronaugh (2013), Climate extremes indices in the CMIP5 multimodel ensemble: Part 1. Model evaluation in the present climate, *J. Geophys. Res. Atmos.*, *118*, 1716–1733, doi:10.3354/cr01221.

Stevens, B., et al. (2013), Atmospheric component of the MPI-M Earth System Model: ECHAM6, *J. Adv. Model. Earth Syst.*, *5*, 146–172, doi:10.1002/jame.20015.

Sueyoshi, T., et al. (2013), Set-up of the PMIP3 paleoclimate experiments conducted using an Earth system model, MIROC-ESM, *Geosci. Model Dev.*, *6*, 819–836, doi:10.5194/gmd-6-819-2013.

Tarasov, L., and W. R. Peltier (2002), Greenland glacial history and local geodynamic consequences, *Geophys. J. Int.*, *150*, 198–229, doi:10.1046/j.1365-246X.2002.01702.x.

Tarasov, L., and W. R. Peltier (2003), Greenland glacial history, borehole constraints, and Eemian extent, *J. Geophys. Res.*, *108*, 1–20, doi:10.1029/2001JB001731.

Tarasov, P. E., O. Peyron, J. Guiot, S. Brewer, V. S. Volkova, L. G. Bezusko, N. I. Dorofeyuk, E. V. Kvavadze, I. M. Osipova, and N. K. Panova (1999), Last Glacial Maximum climate of the former Soviet Union and Mongolia reconstructed from pollen and plant macrofossil data, *Clim. Dyn.*, *15*, 227–240.

Ullman, D. J., A. N. LeGrande, A. E. Carlson, F. S. Anslow, and J. M. Licciardi (2014), Assessing the impact of Laurentide Ice Sheet topography on glacial climate, *Clim. Past*, *10*, 487–507, doi:10.5194/cp-10-487-2014.

Yukimoto, S., et al. (2012), A new global climate model of Meteorological Research Institute: MRI-CGCM3—Model description and basic performance, *J. Meteorol. Soc. Jpn.*, *90A*, 23–64.

Zhang, L., and C. Wang (2013), Multidecadal North Atlantic sea surface temperature and Atlantic meridional overturning circulation variability in CMIP5 historical simulations, *J. Geophys. Res. Oceans*, *118*, 5772–5791, doi:10.1002/jgrc.20390.